PAPER

Check for updates

Rose bengal-integrated electrospun polyacrylonitrile nanofibers for photodynamic inactivation of bacteria†

Xiuli Dong,‡[a] Dionne G. Mitchell,[a] Martha Y. Garcia Cervantes,[a] Basant Chitara,[a] Liju Yang [b] and Fei Yan [*a]

Electrospun polyacrylonitrile (PAN) nanofibers integrated with different loadings of the photosensitizer rose bengal (RB) were synthesized for photodynamic inactivation of bacteria. Our results suggest that the ionic strength in the medium does not significantly affect the RB release from the RB-integrated electrospun PAN nanofibers (RBiEPNs), which could release RB effectively in phosphate-buffered saline (PBS), physiological saline (0.85% NaCl), and deionized H_2O. However, the pH of the medium significantly influenced the release of RB. A larger amount of RB was released in PBS at a higher pH (RB release: pH 9.0 > pH 7.4 > pH 5.0). The RBiEPNs depicted high antimicrobial efficacy against both Gram-negative *Escherichia coli* (*E. coli*) and Gram-positive *Bacillus subtilis* (*B. subtilis*) bacteria under white light irradiation. The antimicrobial efficacy was potent and immediate against the bacterial cells, especially *B. subtilis*. The RBiEPNs containing 0.33 wt% RB demonstrated complete bacterial kills for *B. subtilis* and *E. coli* cells with log reductions of 5.76 and 5.94 in 30 s and 40 min, respectively. The generation of intracellular reactive oxygen species (iROS) was examined after white light treatment of the bacterial cells in the presence of the RBiEPNs. A significant correlation was found between the amount of iROS and the antimicrobial efficacy of the RBiEPNs. The high antimicrobial efficacy could be attributed to several factors, such as the encapsulation efficiency, loading capacity, and RB release behavior of the RBiEPNs, the presence of white light, and the generation of iROS. Taken together, the facile incorporation of a photosensitizer into polymeric nanofibers *via* blend electrospinning offers a feasible strategy for water disinfection.

Environmental significance

Microbial contamination poses a serious risk in water resources worldwide. Despite considerable progress on the development of innovative water treatment technologies, inexpensive and field-deployable strategies are still urgently needed to address this public health issue. In this work, electrospun polyacrylonitrile nanofibers with different loadings of the photosensitizer rose bengal (RB) were synthesized *via* one-step blend electrospinning. The as-prepared RB-functionalized nanofibers depicted high antimicrobial efficacy against both Gram-negative *Escherichia coli* and Gram-positive *Bacillus subtilis* bacteria under white light irradiation. Our results suggest that the incorporation of photosensitizers into electrospun polymer nanofibers provides a very promising solution for water disinfection.

Introduction

One of the biggest challenges facing humanity is the availability of clean and affordable water.[1] In many developing countries, sanitation is a big problem and no access to clean water is common. Contaminated water and poor sanitation cause

[a]*Department of Chemistry and Biochemistry, North Carolina Central University, Durham, NC 27707, USA. E-mail: fyan@nccu.edu; xdong1@nccu.edu*

[b]*Department of Pharmaceutical Sciences, North Carolina Central University, Durham, NC 27707, USA*

† Electronic supplementary information (ESI) available. See https://doi.org/10.1039/d2va00166g

‡ Current address: School of Osteopathic Medicine, Campbell University, Lillington, NC 27546.

disease transmissions. The World Health Organization (WHO) reported that globally, at least 2 billion people use faeces-contaminated drinking water sources, which pose the greatest risk to human health.[1] Pathogens in drinking water with faecal origin (known as enteric pathogens) have caused many illnesses[2] and lead to ~485 000 diarrhoeal deaths each year.[1] A number of waterborne gastroenteritis outbreaks have been caused by diarrhoeagenic *Escherichia coli* (*E. coli*), which has been detected in various ecological niches ranging from mammalian intestines to aquatic environments.[3] The other waterborne pathogenic bacteria include *Salmonella typhimurium*, *Vibrio cholerae*, *Campylobacter jejuni*, *etc.*[4]
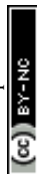
A wide variety of techniques have been developed to remove or inactivate bacteria in water, such as the use of wetland

systems,[5] filters,[6,7] flocculants,[8] antimicrobial reagents,[8,9] Cu_2O-contained hybrids,[10,11] antimicrobial nanofibers,[12] *etc.* Cu_2O-contained hybrids, including Cu_2O particles on inorganic halloysite nanotubes and on tourmaline, have been reported as a promising antimicrobial technology to inactivate bacteria completely within a short time.[10,11] However, antimicrobial nanofibers produced by electrospinning exhibit several advantages over others, including ease of preparation, efficient synthesis procedure, cost-effectiveness, *etc.* The electrospinning process uses a high voltage electric field to produce electrically charged jets from polymer solutions or melts and create nanofibers by evaporation of the solvent, followed by a fibre collection step through directing the highly charged fibres towards the oppositely charged collector by the electric field.[13] The electric field plays a key role in the electrospinning process for mass production of nanofibers. It was observed that the morphology and diameters of nanofiber could be adjusted by changing the needle distance and the applied voltage, which may further influence the mechanical performance of the nanofiber yarn.[14] Compared to conventional fibres' structures, electrospun nanofibers show promising properties, such as lightweight with small diameters, controllable pore structures, and large surface area/volume ratio.[15] These properties make them ideal for the use in making filters, sensors, and protective clothing, and for the application in tissue engineering, functional materials, and energy storage.[15,16] For instance, the application of electrospun nanofibers on tissue engineering produced extracellular matrix-biomimetic structures with better biocompatibility.[17,18] Nanofibers can be modified by the incorporation of different compounds to endow certain functions. In biomedical field, the nanofibers have been loaded with many bioactive substances, such as proteins, peptides, and small molecule drugs for drug delivery.[18,19]

Many types of polymers have been used to make electrospun nanofibers, including cellulose acetate, acrylic resin, polyethylene oxide, polyethylene terephthalate, polyacrylonitrile (PAN), *etc.*[13] Among them, PAN has been widely used for making nanofibers for filtration and for making wound dressing due to its unique characteristics, such as high mechanical strength, excellent thermal stability, chemical inertness, light resistance, non-toxicity, and electrospinability.[20–23] PAN can be effectively used in nanocomposites and carbon fibre production, and can also be used in a copolymer form for fibre productions.[24]

To produce antimicrobial electrospun nanofibers, antimicrobial components can be integrated into nanofibers during the electrospinning procedure. The antimicrobial effects were observed from electrospun nanofibers integrated with silver nanoparticles (Ag NPs),[25] chitosan-silver NPs,[16] graphene oxide,[26] cinnamaldehyde,[27] antimicrobial peptides,[28] *etc.* RB is a hydrophilic photosensitizer (PS) with a high absorption coefficient in the visible region of the solar spectrum showing good quantum yield of singlet oxygen,[29] it has been used in the photodynamic therapy (PDT) for cancer treatment due to its efficiency in cell death induction and high selectivity for tumour cells.[30] RB has also emerged as a promising alternative to antibiotics for the inactivation of multidrug resistant pathogens.[31] Studies have shown that a high-purity form of RB (>99.5% dye content) can kill

a battery of G^+ bacteria, including drug-resistant strains at low concentrations (0.01–3.13 μg mL^{-1}) under fluorescent, LED, and natural light in a few minutes.[32] RB can also eradicate bacterial biofilms and the development of RB-resistance in bacteria is extremely low (less than 1×10^{-13}).[32]

In this work, electrospun PAN nanofibers with different loadings of RB were synthesized *via* one-step blend electrospinning. The as-prepared nanofibers were characterized by scanning electron microscopy (SEM), attenuated total reflectance Fourier transform infrared spectroscopy (ATR-FTIR), UV-vis absorption spectroscopy. To the best of our knowledge, no prior study has reported the antimicrobial activity of RB integrated electrospun nanofibers, and this is the first time that different amounts of RB were integrated into PAN nanofibers by one-step blend electrospinning for photodynamic inactivation of bacteria. The as-prepared RB-integrated electrospun PAN nanofibers or RBiEPNs have the potential to inactivate bacteria in the contaminated water.

Materials and methods

Materials and reagents

Polyacrylonitrile (PAN), with a molecular weight of 150 000 dalton was purchased from Sigma Aldrich (St. Louis, MO). *N,N*-Dimethylformamide (DMF, 99.9%), rose bengal, dihydrorhodamine (DHR) 123, and NaCl were purchased from Thermo Fisher Scientific, (Waltham, MA). *Escherichia coli* (*E. coli*, Gram-negative or G^- bacteria, K12) and Gram-positive or G^+ *Bacillus subtilis* (*B. subtilis*) were purchased from the American Type Culture Collection (ATCC; Manassas, VA). The power supply was from Gamma High Voltage Research (ES40P-20 W/DA), the syringe pump was from KD Scientific (KDS-100), and the dehumidifier from Comfort-Air (BHD-301-H). All bacteria samples were handled and disposed of using appropriate biosafety guidelines.

Synthesis of RBiEPNs *via* one-step blend electrospinning

The spinning solution was prepared by adding 1.62 g PAN into 15 mL DMF followed by mechanical stirring at 1000 rpm overnight at ambient temperature until a homogeneous solution was achieved. Subsequently, appropriate amount of RB (0.16 wt%, 0.33 wt%, or 0.49 wt%) was dissolved in the homogeneous PAN solution by stirring for 2 h. The solution was then transferred into a 12 mL plastic syringe equipped with a 21-gauge blunt probe needle. When the electrospinning process was performed, a DC voltage of 15 kV was applied, the tip to collector distance was set as 13 cm, and the flow rate of the syringe pump was set at 0.6 mL h^{-1}. The collector was a round 20 cm aluminium plate covered with aluminium foil. Electrospinning was allowed to continue until all 12 mL of solution were dispensed. The resulting membrane was carefully peeled from the collection plate for further analysis and subsequent treatment.

Characterization of RBiEPNs

SEM images were examined by an FEI Verios 460L SEM. FTIR spectra were collected with a NICOLET iS5 spectrometer from

© 2022 The Author(s). Published by the Royal Society of Chemistry

Environ. Sci.: Adv., 2022, **1**, 736–745 | **737**

Thermo Scientific, Inc. Each spectrum was collected in the range 1000–3500 cm^{-1}.

RB release test

The RBiEPNs were cut to the size about 1 cm × 1 cm (~2.4 mg) for all the tests in this study. To test the effect of RB loading on the RB release, the RBiEPNs with different loadings were placed in 5 mL phosphate-buffered saline (PBS, pH 7.4), which was used as RB release medium. The tubes were wrapped with aluminium foil to avoid light irradiation and were placed on a shaker (Lab-Line Instruments, Inc., IL) at the setting of 2. Different sampling time was used and the optical densities (OD) of the samples were measured at the wavelength 562 nm using SpectraMax M5 multi-detection reader with the software SoftMax Pro5.4.5 (Molecular Devices Corp., CA). To test the effect of ionic strength on the RB release, three release media were used, these include: de-ionized water (DI-H$_2$O), PBS (pH 7.4), and 0.85% NaCl solution. To test of the effect of the pH on RB release, the release media were PBS with a pH of 5.0, 7.4, and 9.0.

Antimicrobial assay

E. coli K12 or *B. subtilis* bacteria cells were freshly grown overnight in tryptic soy broth (TSB) at 37 °C on a shaker before each test. The cells were collected and the broth was removed by centrifugation, followed by washing with PBS (pH 7.4) twice and re-suspended in PBS. The cells were then diluted to the concentration of ~1.2 × 10^7 colony-forming unit (cfu) mL^{-1} for the treatment.

50 μL of bacterial cells were placed on top of the surface of the RBiEPNs containing different amounts of RB. The samples were exposed to the white light (60 W) for light treatment or kept in the dark for dark treatment at different times. Electrospun PAN nanofibers without RB were used as controls (EPNs). After the treatment, each sample was placed into a 1.5 mL-centrifuge tube containing 950 μL PBS. The tubes were vigorously vortexed in the dark for 3 min to release the cells. To test viable cell numbers, ten-fold serial dilutions were made in PBS (pH 7.4) and the cells were spread on tryptic soy agar (TSA) plates. The colony number was counted after 18 h at 37 °C in the dark. The decrease of viable cell numbers by RBiEPN was due to the antimicrobial effects.

Quantitation of intracellular ROS

150 μL of *E. coli* and *B. subtilis* cells were placed on RBiEPNs containing 0.33 wt% RB. The samples were exposed to white light with different times and then were immersed into 900 μL PBS. The cells were washed off from RBiEPNs by vigorously vortexed for 3 min. The cell suspensions were transferred into new centrifuge tubes and the RBiEPNs were discarded. To remove RB from the cells, the cell suspensions were centrifuged at 9000 rpm for 5 min, the supernatants were removed, and then the cells were washed once with 0.85% NaCl solution by centrifugation and were re-suspended in 350 μL of 0.85% NaCl solution. The cells were equally split into two tubes, one for staining and another one as blank. To stain the cells, 175 μL of 2 μM dihydrorhodamine 123 (DHR 123) in 0.85% NaCl solution was added into the cell suspension. As for the blanks, 175 μL of

0.85% NaCl solution without the dye was added. The cells were incubated at the room temperature in the dark for 40 min. After centrifugation, the supernatants were removed, the cells were washed once with 0.85% NaCl solution and re-suspended in 320 μL of 0.85% NaCl solution. The fluorescence intensities (excitation 500 nm and emission 535 nm) were measured using the SpectraMax M5 microplate reader. The increase of fluorescence intensity compared with the controls (no light treatment) was considered the ROS generation in bacteria by RBiEPNs treatment in the presence of light.

Results and discussion

Morphological characterization

Fig. 1 depicts the SEM images of the RBiEPNs containing different amounts of RB. All three samples showed similar fibre morphology. While the entrapment of RB dye molecules had little apparent effect on the inner diameter of the resulting nanofibers, the surface roughness increased for electrospun PAN nanofiber with a 0.49 wt% loading of RB (Fig. 1c), which could be due to the slight increase in viscosity of the precursor solution at a higher RB concentration. The XRD pattern for electrospun PAN nanofibers did not show any phase changes after the incorporation of different amounts of RB, as shown in Fig. S1, ESI†

FTIR spectral analysis

Fig. 2 displays the FTIR spectra of the RB dye, pure electrospun PAN nanofibers, and the RBiEPNs containing 0.49 wt% RB. In the FTIR spectrum of neat RB powder (Fig. 2a), the absorption peak near 1614 cm^{-1} could be attributed to carbonyl stretching (=C–O) vibrations. The adsorption peaks at 2919 and 2848 cm^{-1} could be attributed to the vibrations due to =C–H stretching, and the other three strong peaks in the ranges of 1300–1600 cm^{-1} correspond to the C=C stretching vibrations.[33] In the FTIR spectrum of electrospun PAN nanofibers (Fig. 2c), the stretching vibration of C≡N in PAN was observed at the peak of 2245 cm^{-1}. The stretching vibrations of C=O and the bending vibrations of C–H were found in the ranges of 1730–1737 cm^{-1} and 1455–1460 cm^{-1}, respectively.[34] The distinctive characteristic vibrational band of 1565 cm^{-1} of RB was detected in the RBiEPNs containing 0.49 wt% RB (Fig. 2b), indicating that RB was successfully incorporated into the PAN nanofibers.

RB release profiles in PBS (pH 7.4)

Fig. 3 illustrates the RB release profiles from the RBiEPNs containing different amounts of RB in a pH 7.4 PBS buffer solution. The RB release was immediate and RB was detectable
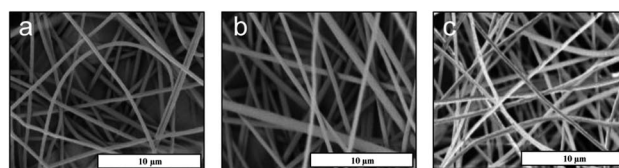

Fig. 1 SEM images of electrospun PAN nanofibers loaded with (a) 0.16 wt% RB, (b) 0.33 wt% RB, and (c) 0.49 wt% RB. Scale bar: 10 μm.
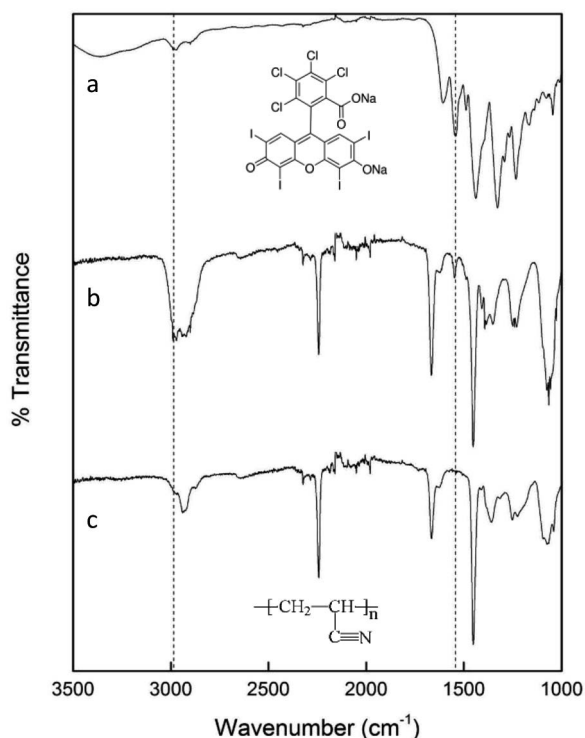
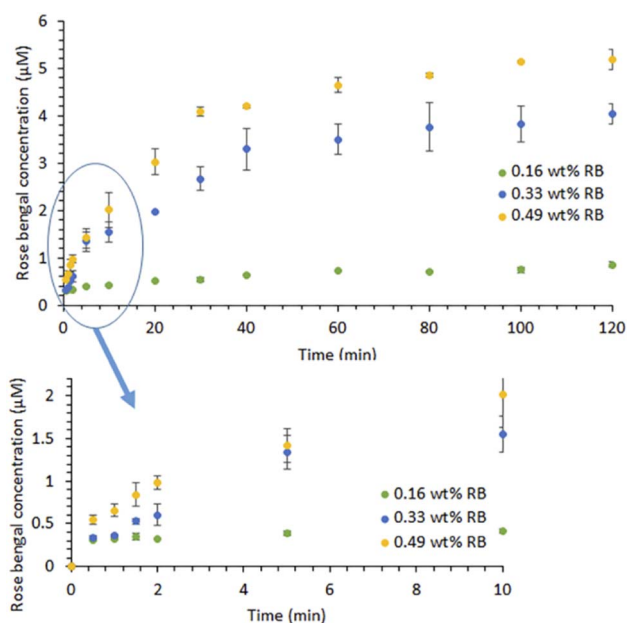Fig. 2 FTIR spectra of (a) neat RB powder, (b) the RBiEPNs containing 0.49 wt% RB, and (c) electrospun PAN nanofibers.

Fig. 3 RB release profiles of the RBiEPNs in PBS (pH 7.4) in the dark. Data is presented as mean values of triplicate measurements with ±standard deviation (SD) error bars.

in PBS within 30 s, suggesting that many RB molecules were on or near the fibre surface. At the same release time, a larger amount of RB was released from the RBiEPNs containing higher loading of RB. For instance, after 10 min release time the RB concentrations in PBS were 0.41, 1.55, and 2.01 μM from the

RBiEPNs containing 0.16 wt%, 0.33 wt%, and 0.49 wt% RB, respectively. The RB concentration increased rapidly during the first 10 min, after which the concentration slowly increased. In the case of the RBiEPNs containing 0.49 wt% RB, the RB5 concentration increased 267.66% and 0.88% from the time 0.5 min to 10 min, and from the time 100 min to 120 min, respectively. The initial burst release within the first 10 min is most likely linked to weakly bound or adsorbed RB molecules to the surface of the RBiEPNs. The release behaviour during the sustained release stage could be explained by the diffusion-mediated dissociation of RB from the RBiEPNs.

Similar release patterns were observed in many compound-loaded electrospun nanofibers by others.[35–37] Severyukhina et al.[35] fabricated chitosan-based nanofibers containing the PS Photosens by electrospinning and studied Photosens release profiles in PBS during a 96 h period. The authors observed that Photosens' release profiles contained a burst release during the first 24 h and a sustained release thereafter.[35] Zong et al. prepared poly(lactic acid) (PLA) electrospun fibres containing Mefoxin and observed a burst release of Mefoxin in the first 3 h, and a complete release within 48 h.[38] Samadi et al.[37] incorporated graphene oxide/TiO$_2$/doxorubicin (GO/TiO$_2$/DOX) complex in electrospun chitosan/PLA nanofibers and observed initial burst release of DOX and subsequent sustained release from the nanofibers with the thicknesses of 30 and 50 μm. The authors indicated that the thickness and the density of nanofibers affected drug release, showing that the thicker nanofibers reduced the DOX release rate and the drug diffusion from the pores of nanofibers was a predominant reaction for DOX release from nanofibers with thicknesses of 30 and 50 μm.[37] The duration of the initial burst release stage in our study was much shorter than those observed by others.[35,37] It was known that the selection of compound–polymer–solvent systems determines the burst release of drugs.[39] The difference in the compound type, compound loading, the polymer, and the solvent might explain the difference in release profiles between our study and those done by others.

In our present study, the RB release profiles from the RBiEPNs could be approximated by the Peppas equation:[35,40,41]

$$Q = kt^n \tag{1}$$

where Q is the cumulative RB dye release, t is the release time (min), k is a constant related to the geometry and the structure of the electrospun PAN nanofibers, and n is a coefficient related to the mechanism and kinetics of the release of RB.[40,41]

The kinetic parameter "n" was found to be 0.21, 0.50, and 0.38 for the RBiEPNs containing 0.16, 0.33, and 0.49 wt% RB, respectively (see Table 1), suggesting Fickian diffusion is the dominant mechanism for the release of RB from the electrospun PAN nanofibers.[34]

Effect of ionic strength and pH on the RB release

The effect of different media ionic strengths and pH on the RB release kinetics was studied. Fig. 4A shows that RB was released effectively from the RBiEPNs containing 0.33 wt% RB into these three media within 120 min. A slightly larger amount of RB was released in PBS (pH 7.4) than in 0.85% NaCl solution or DI-H$_2$O

© 2022 The Author(s). Published by the Royal Society of Chemistry

Environ. Sci.: Adv., 2022, **1**, 736–745 | **739**

at all the sampling times. The kinetic parameter "n" was found to be 0.41, 0.47, and 0.40 for the release of RB from the RBiEPNs containing 0.33 wt% RB in DI-H_2O, 0.85% NaCl solution and PBS (pH 7.4), respectively (see Table 2). This observation was different from what was reported by others, which demonstrated a much higher PS (Photosens) release from chitosan-based nanofibers in PBS (pH 7.4) than in distilled H_2O (pH 5.5).[35] This discrepancy might be due to the differences on the pH of DI-H_2O, the characteristics of the loaded compounds, the lipophilicity of the polymers used for nanofiber synthesis, *etc.*

The pH of the release medium showed a significant effect on RB release. Fig. 4B shows that PBS at a higher pH favoured RB release. As the pH of the release medium increases, faster kinetics is observed as indicated by slightly higher "n" values during the first 30 min as shown in Table 3. The kinetic parameter "n" was found to be 0.51, 0.52, and 0.55 for the release of RB from the RBiEPNs containing 0.33 wt% RB in PBS solution at pH 5.0, pH 7.4, and pH 9.0, respectively. It was possible that the interaction between RB and PAN decreased with the increasing of the pH in the environment. Similar observations were reported by others.[42,43] Sayin *et al.*[42] synthesized RB-loaded water-soluble polyvinyl alcohol (PVA) nanofibers with a thin layer of poly(4-vinylpyridine-*co*-ethylene glycol dimethacrylate) p(4VP-*co*-EGDMA) coating and found that RB released more at pH 6.5 and pH 9 than pH 4, showing the RB release was proportional to the pH of the solution. Gupta *et al.*[43] observed that RB adsorption on the bottom ashes from the furnace decreased with the increase of pH, and the dilute NaOH solution could release 91% of the adsorbed RB from the ashes, suggesting that alkaline solutions were suitable for RB release. The other important factor besides pH that might affect RB releases was the structure of nanofibers, including the fibre diameter, density, thickness, and the pore size.

It should be noted that the Peppas model is semi-empirical, and it is only suitable for studying release kinetics up to 60% of release.[44] In this study, the fit parameters obtained are mainly used to interpret the effect of the ionic strength and the pH on the release kinetics and provide insights into the dominant mechanism, as opposed to thoroughly explaining the active mechanisms associated with the release. Deviations from the model may occur due to the possible dissolution or swelling of the polymer itself, the difference in the porosity and surface morphology of electrospun polymers in the presence of different amounts of RB, or the aggregation of RB dye molecules at high concentrations *etc.*

Antimicrobial efficacy testing

To test the effect of light exposure on bacteria, *E. coli* K12 cells with a total number of 6.33×10^5 were treated with the RBiEPNs
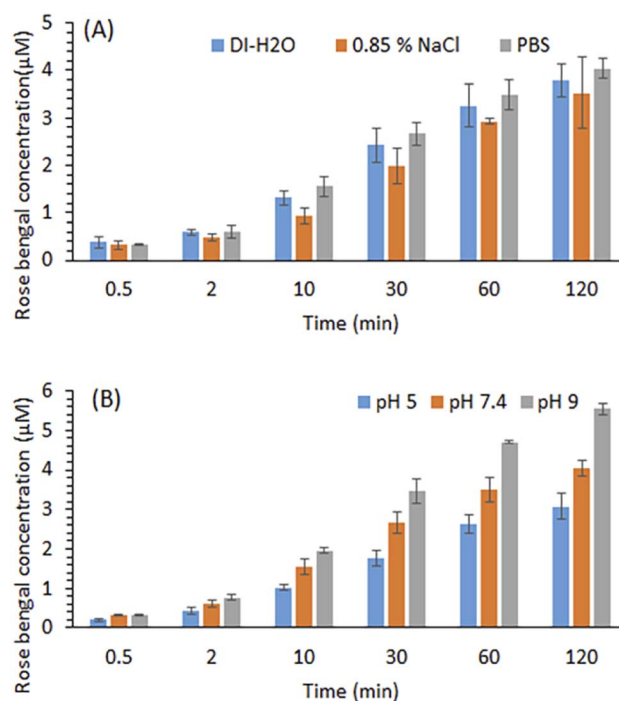

Fig. 4 Effects of ion (A) and pH in PBS (B) on the RB release from the RBiEPNs containing 0.33 wt% RB in the dark. Data is presented as mean values of triplicate measurements with ±SD error bars.

containing 0.49 wt% RB under the light or in the dark for 0, 30, or 60 min. The electrospun PAN nanofibers (EPNs) in the absence of RB were used as controls. Fig. 5 shows that EPNs alone did not change the viable cell numbers even after 60 min treatment compared to the initial cell numbers, indicating that (i) EPNs did not have antimicrobial effects on *E. coli* cells, and (ii) *E. coli* cells did not have strong affinity to EPN surfaces and were completely released from EPNs into PBS. Similar to the results of the control study, the dark treatment on RBiEPNs did not show obvious antimicrobial effects on *E. coli* cells. When the light was present, RBiEPNs were highly effective to inactive *E. coli* cells, showing a complete killing effect with 60 min light treatment time. RBiEPNs caused 3.65 and 5.80 log reductions of total cell numbers with the treatment time of 30 and 60 min, respectively.

The antimicrobial effects of the RBiEPNs with different RB loadings were tested against both *E. coli* and *B. subtilis* cells under white light irradiation at various times. Fig. 6 shows that the antimicrobial efficacy of the RBiEPNs was dependent on the amount of RB-loading and the duration of light treatment. With the same treatment time, the RBiEPNs with higher RB loadings

Table 1 Peppas parameters of RB release profiles in PBS (pH 7.4)

RBiEPNs samples	R^2	k	N
0.16 wt% RB	0.98	0.29	0.21
0.33 wt% RB	0.98	0.47	0.50
0.49 wt% RB	0.98	0.92	0.38

Table 2 Peppas parameters of RB release profiles in media with different ionic strength

Release medium	R^2	k	N
DI H_2O	0.9918	0.56	0.41
0.85% NaCl	0.9919	0.39	0.47
PBS (pH 7.4)	0.9906	0.63	0.40

Table 3 Peppas parameters of RB release profiles in PBS buffer at different pH during the first 30 min

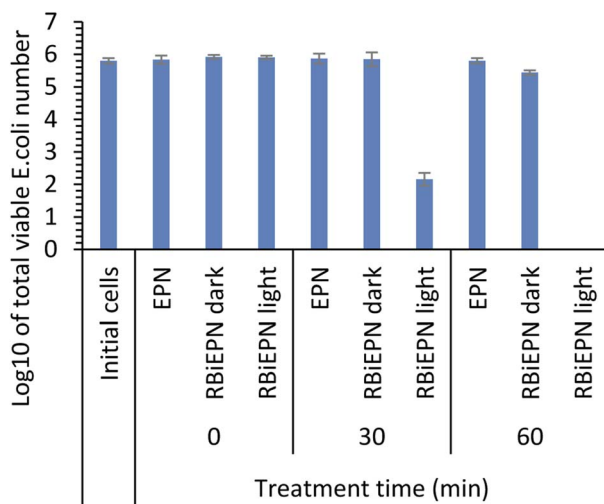| pH	R^2	k	N
5.0	0.9998	0.31	0.51
7.4	0.9993	0.46	0.52
9.0	0.9996	0.54	0.55

Fig. 5 Antimicrobial effects of electrospun PAN nanofibers in the absence of RB (EPNs) and with a loading of 0.49 wt% RB (RBiEPNS) on *E. coli* K12 cells. Data is presented as mean values of triplicate measurements with ±SD error bars.

Fig. 6 Antimicrobial effect of the RBiEPNs on *E. coli* K12 cells (A) and *B. subtilis* (B) cells with different treatment time under white light irradiation. Data is presented as mean values of triplicate measurements with ±SD error bars.

showed higher antimicrobial effects. For instance, with a 40 min light treatment, the RBiEPNs containing 0.33 wt% RB completely inactivated *E. coli* cells, showing 5.94 log reductions of cell numbers, whereas the RBiEPNs containing 0.16 wt% RB caused 3.58 log reductions of cell numbers and did not show a complete killing effect (Fig. 6A). Similarly, the RBiEPNs with the same RB loadings showed higher antimicrobial efficacy with a longer light treatment. The log 10 values of viable *E. coli* cell numbers after being treated with the RBiEPNs containing 0.49 wt% RB were 5.66, 4.84, 3.11, and 0 with a treatment time of 10, 20, 30, and 40 min, respectively. At the treatment time 60 min, even the RBiEPNs containing 0.33 wt% RB showed a complete killing effect. *B. subtilis* cells were much more vulnerable to the RBiEPNs than *E. coli* cells. Although RBiEPNs treatments in the dark did not show antimicrobial effects on *E. coli* cells, they showed antimicrobial effects on *B. subtilis* cells (at light treatment time 0), especially the RBiEPNs with 0.49 wt% RB loading (Fig. 6B).

One of the goals of this study was to test the application potential of RBiEPNs to inactivate the microorganisms in water. Water has different pH values in nature. Knowing the pH effect on RBiEPNs can help us optimize the treatment condition. As shown in Fig. 4B, the RB release was affected by the pH value. PBS with a higher pH value caused more RB release at a given time. Since the antimicrobial effects from RB are at a concentration-dependent mode, displaying that a higher RB release
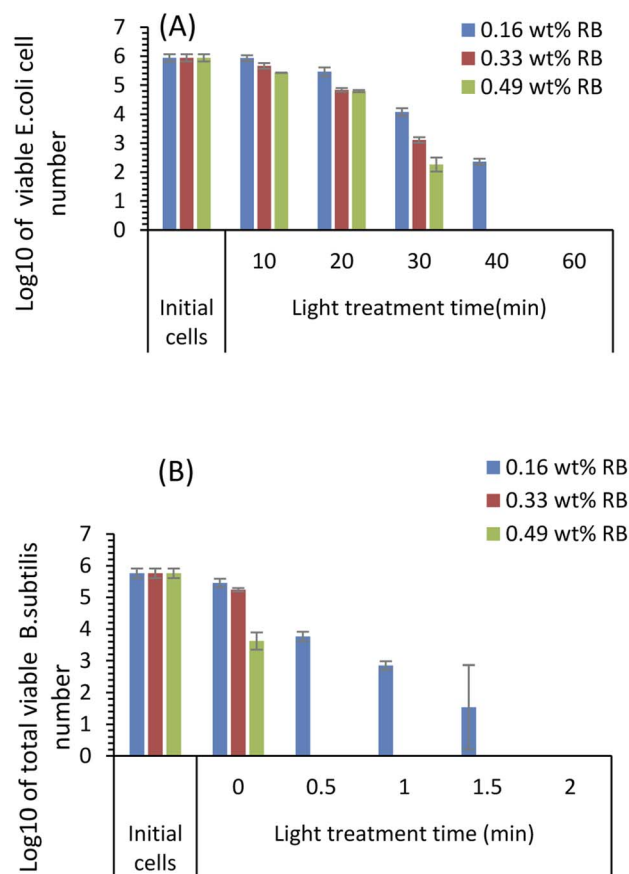
from, or a higher RB loading in, RBiEPNs showed higher antimicrobial effects (Fig. 6), we can deduce that RBiEPNs are more effective to inactivate bacteria at neutral or alkaline conditions than at acidic conditions due to more RB release.

The effectiveness of RB release from the RBiEPNs during bacterial treatments could explain the observed antimicrobial effects. The antimicrobial efficacy of RB has been widely accepted and used to photo-inactivate various types of bacteria including multidrug resistant bacteria and biofilms.[31,32] It was reported that the minimal bactericidal concentrations of RB with a high-purity form (>99.5% dye content) on *B. subtilis* ATCC6051, *E. faecium* NR-32065, and *E. coli* 35218 under the light were 0.02, 0.78, and 1.6 µg mL^{-1}, respectively.[32]

The RBiEPNs displayed much higher antimicrobial efficacy against G$^+$ *B. subtilis* than G$^-$ *E. coli*. This might be due to the difference in their cell envelope structures. The G$^-$ bacterial cell envelope contains the outer membrane, the peptidoglycan cell wall, and the inner membrane.[46] The outer membrane plays a major role in protecting G$^-$ bacteria from the environment by excluding toxic molecules and providing an additional stabilizing layer around the cell.[46] The outer membrane can reduce the degree of PS permeability and contribute to PDI resistance.[47,48] As for the G$^+$ bacterial cell envelope, there is no outer membrane but

© 2022 The Author(s). Published by the Royal Society of Chemistry

Environ. Sci.: Adv., 2022, **1**, 736–745 | **741**

multiple layers of peptidoglycan.[46] The absence of outer membrane in G[+] bacteria might be the major reason that G[+] *B. subtilis* cells were much more vulnerable to RB than G[−] *E. coli* cells. Silva *et al.*[48] observed that the photo-killing process by RB and erythrosine with green LED light changed the surface properties of the bacterial cells and induced potassium (K^{−}) leakage.[48] K^{+} leakage from G[+] bacteria was higher than G^{−} cells. G[+] bacteria such as *S. aureus*, *L. innocua*, and *E. hirae* were more vulnerable to photosensitization than G[−] *E. coli* cells.[48] Other studies also reported that higher PS concentrations or longer irradiation times were needed to inactivate G[−] bacteria.[31,49]

The antimicrobial efficacy of the RBiEPNs was much higher and more immediate than those reported by others. For instance, chitosan-based electrospun nanofibers (1 cm[2]) reduced bacterial growth of 99.93% *E. coli*, 99.9% *L. innocua*, 99.14% *S. aureus*, and 96.81% *S. typhimurium* after 4 h incubation in PBS.[50] Electrospun poly(ether amide) nanofibers containing Ag NPs inhibited >99.9% *E. coli* and *S. aureus* with 24 h treatment time.[51] The cationic starch nanofibers loaded with carvacrol@casein NPs reduced *B. cereus* by 2 log cfu g[−1].[52]

Quantitation of intracellular ROS generation in *B. subtilis* and *E. coli*

DHR 123 was used as an indicator for intracellular ROS (iROS) generation in *E. coli* and *B. subtilis* bacterial cells. DHR 123 is an uncharged and non-fluorescent ROS indicator, which can passively diffuse across membranes, be oxidized to cationic rhodamine 123 in the mitochondria, and exhibit green fluorescence. Our results showed that after bacteria being placed on the surface of the RBiEPNs containing 0.33 wt% RB and exposed to white light, the iROS was generated immediately and increased with the increasing of the treatment time, especially in *B. subtilis* (Fig. 7).

The level of iROS in *B. subtilis* increased 93.03% after a 30 s light exposure and further increased to 119.2% after a 4 min light exposure compared to the controls. This explained the complete killing effect after a 30 s treatment from the aforementioned results. The iROS generation in *E. coli* cells was also observed, although the level was lower than that observed in *B. subtilis*, even with much longer treatment time. The level of iROS in *E. coli* cells increased 27.11% and 76.28% after a 10 and 40 min light treatment, respectively. The higher iROS generation in *B. subtilis* than in *E. coli* was correlated with the observation that *B. subtilis* cells were more vulnerable to the RBiEPNs than *E. coli* cells. In general, the mechanisms of photodynamic inactivation of bacteria are as follows. The photosensitizing molecules bind to bacterial cell walls, or penetrate through cell walls.[53] In the presence of light, the photosensitizing molecules are excited and energies are transferred from these molecules to dissolved molecular oxygen, leading to the formation of ROS.[31,54] The ROS can irreversibly damage bacterial cells, cause protein oxidations, lipid peroxidation, and nucleic acid damages, and eventually lead to cells' death.[31,54,55] As for the PDT on cancer cells, the quantum yield of ROS generation from the photosensitizing molecules significantly influences the PDT efficiency in cancer cells.[45]
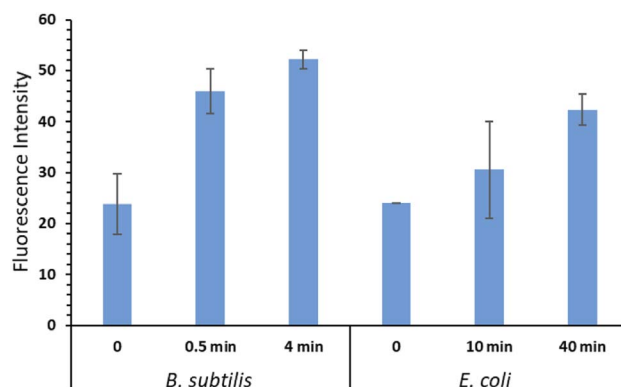

Fig. 7 Fluorescence intensities from iROS generated in *B. subtilis* cells and *E. coli* cells after treated on the surface of the RBiEPNs containing 0.33 wt% RB under white light irradiation. Data is presented as mean values of triplicate measurements with ±SD error bars.

There were two pathways of ROS generation in PDT. The type I pathway mainly generates superoxide radicals ($O_2^{\bullet-}$), hydroxyl radicals ($^{\bullet}OH$), and other cytotoxic ROS through hydrogen or electron transfer.[56,57] The type II pathway, on which most of the PDTs related to clinical applications are based, generates singlet oxygen ($^1O_2$).[56,57] RB is a well-known type II PS and forms $^1O_2$.[30]

$^1O_2$ is the most important reactive species in PDT-mediated cytotoxicity.[30] $^1O_2$ diffuses freely through cells and can cross cell membranes. For instance, Skovsen *et al.*[58] created $^1O_2$ in a single nerve cell upon irradiation of a PS (5,10,15,20-tetrakis(*N*-methyl-4-pyridyl)-21*H*,23*H*-porphine) incorporated in the cell nucleus using a focused laser beam, and observed that a significant fraction of $^1O_2$ formed in the nucleus is able to diffuse over appreciable distances including across the cell membrane into the extracellular medium.

The iROS generated by RB in this study could come from two major sources: (i) a direct diffusion of $^1O_2$ from the extracellular environment through the damaged cell walls and cell membranes, and (ii) an influx of $^1O_2$ being produced intracellularly through RB penetration. It is highly possible that due to the difference in the bacterial cell envelope structure between *E. coli* cells and *B. subtilis* cells, the penetrations of RB and $^1O_2$ into the cells were deeper in *B. subtilis*, leading to higher intracellular $^1O_2$ levels in *B. subtilis* cells.

The oxygen supply in the environment is considered as a crucial factor in the efficacy of photodynamic inactivation of bacteria,[59] the other factors include the light source, the type of the PS, and the penetration depth of light into the treatment medium or tissue.[60] Our results suggest that the RBiEPNs effectively produced $^1O_2$ through the activation of RB under white light irradiation, and the RBiEPNs were highly effective for bacteria inactivation.

Conclusions

The RBiEPNs containing different amounts of RB could effectively release RB in DI-H$_2$O, PBS, and 0.85% NaCl solution. The ionic strength did not significantly affect the release of RB. However, the RB release was significantly influenced by the pH

742 | *Environ. Sci.: Adv.*, 2022, **1**, 736–745

© 2022 The Author(s). Published by the Royal Society of Chemistry

of the release medium and was accelerated with the increasing of the pH. The RBiEPNs were highly effective to inactivate both G^+ *B. subtilis* and G^- *E. coli* bacteria under white light irradiation. The killing effects were potent and immediate, especially against *B. subtilis*. The RBiEPNs containing 0.33 wt% RB displayed a complete killing effect against *B. subtilis* and *E. coli* cells with a log reduction of 5.76 in 30 s and a log reduction of 5.94 in 40 min, respectively. The antimicrobial efficacy of the RBiEPNs was correlated with the amount of iROS, as evidenced by the presence of higher iROS levels in *B. subtilis* cells than in *E. coli* cells. The simplicity and scalability of the electrospinning process, together with the excellent antimicrobial activity of the PS under visible light irradiation make it a feasible strategy for water disinfection.

Author contributions

FY and XD designed this study. XD, DM, MC and BC performed the experiments. XD drafted the manuscript. LY and FY revised the manuscript. All authors accepted to submit for publication.

Conflicts of interest

There are no conflicts to declare.

Acknowledgements

References

1 WHO, *Drinking-water*, 2022, **https://www.who.int/newsroom/fact-sheets/detail/drinking-water**, accessed on August 22, 2022.

2 N. J. Ashbolt, Microbial contamination of drinking water and disease outcomes in developing regions, *Toxicology*, 2004, **198**, 229–238.

3 J. Park, J. S. Kim, S. Kim, E. Shin, K. H. Oh, Y. Kim, C. H. Kim, M. A. Hwang, C. M. Jin, K. Na, J. Lee, E. Cho, B. H. Kang, H. S. Kwak, W. K. Seong and J. Kim, A waterborne outbreak of multiple diarrhoeagenic *Escherichia coli* infections associated with drinking water at a school camp, *Int. J. Infect. Dis.*, 2018, **66**, 45–50.

4 F. Y. Ramirez-Castillo, A. Loera-Muro, M. Jacques, P. Garneau, F. J. Avelar-Gonzalez, J. Harel and A. L. Guerrero-Barrera, Waterborne pathogens: detection methods and challenges, *Pathogens*, 2015, **4**, 307–334.

5 X. L. Dong and G. B. Reddy, Soil bacterial communities in constructed wetlands treated with swine wastewater using PCR-DGGE technique, *Bioresour. Technol.*, 2010, **101**, 1175–1182.

6 A. Sato, R. Wang, H. Y. Ma, B. S. Hsiao and B. Chu, Novel nanofibrous scaffolds for water filtration with bacteria and virus removal capability, *J. Electron Microsc.*, 2011, **60**, 201–209.

7 W. T. Zheng, Y. B. A. Liu, W. Liu, H. D. Ji, F. Li, C. S. Shen, X. F. Fang, X. Li and X. G. Duan, A novel electrocatalytic filtration system with carbon nanotube supported nanoscale zerovalent copper toward ultrafast oxidation of organic pollutants, *Water Res.*, 2021, **194**, 116961.

8 X. L. Dong, W. X. Liang, M. J. Meziani, Y. P. Sun and L. J. Yang, Carbon dots as potent antimicrobial agents, *Theranostics*, 2020, **10**, 671–686.

9 D. L. Guo, S. J. You, F. Li and Y. B. Liu, Engineering carbon nanocatalysts towards efficient degradation of emerging organic contaminants *via* persulfate activation: a review, *Chin. Chem. Lett.*, 2022, **33**, 1–10.

10 Y. P. Wang, Q. Q. Wang, G. Y. Wu, H. X. Xiang, M. T. Innocent, M. Zhai, C. Jia, P. Zou, J. L. Zhou and M. F. Zhu, Ultra-fast bacterial inactivation of Cu_2O@halloysite nanotubes hybrids with charge adsorption and physical piercing ability for medical protective fabrics, *J. Mater. Sci. Technol.*, 2022, **122**, 1–9.

11 J. Zhou, M. Zhai, R. Wang, Y. Wang, Q. Wang, Z. Hu, H. Xiang and M. Zhu, High metal-loaded Cu_2O@TM hybrids for melt-spun antibacterial fibers engineered towards medical protective fabrics, *Composites, Part A*, 2022, **161**, 1–8.

12 S. Rashki, N. Shakour, Z. Yousefi, M. Rezaei, M. Homayoonfal, E. Khabazian, F. Atyabi, F. Aslanbeigi, R. S. Lapavandani, S. Mazaheri, M. R. Hamblin and H. Mirzaei, Cellulose-based nanofibril composite materials as a new approach to fight bacterial infections, *Front. Bioeng. Biotechnol.*, 2021, **9**, 732461.

13 T. Subbiah, G. S. Bhat, R. W. Tock, S. Pararneswaran and S. S. Ramkumar, Electrospinning of nanofibers, *J. Appl. Polym. Sci.*, 2005, **96**, 557–569.

14 S. X. Jin, B. J. Xin, Y. S. Zheng and S. H. Liu, Effect of electric field on the directly electrospun nanofiber yarns: simulation and experimental study, *Fibers Polym.*, 2018, **19**, 116–124.

15 Y. Cai, Q. Wei and F. Huang, in *Functional Nanofibers and Their Applications*, ed. Q. Wei, Woodhead Publishing, 2012, pp. 38–54.

16 N. Bandatang, S. A. Pongsomboon, P. Jumpapaeng, P. Suwanakood and S. Saengsuwan, Antimicrobial electrospun nanofiber mats of NaOH-hydrolyzed chitosan (HCS)/PVP/PVA incorporated with in situ synthesized AgNPs: Fabrication, characterization, and antibacterial activity, *Int. J. Biol. Macromol.*, 2021, **190**, 585–600.

17 L. Jiang, Y. C. Jiang, J. Stiadle, X. F. Wang, L. X. Wang, Q. Li, C. Y. Shen, S. L. Thibeault and L. S. Turng, Electrospun nanofibrous thermoplastic polyurethane/poly(glycerol sebacate) hybrid scaffolds for vocal fold tissue engineering applications, *Mater. Sci. Eng., C*, 2019, **94**, 740–749.

18 K. Q. Ye, H. Z. Kuang, Z. W. You, Y. Morsi and X. M. Mo, Electrospun nanofibers for tissue engineering with drug loading and release, *Pharmaceutics*, 2019, **11**, 182.

19 A. Ghaderpour, Z. Hoseinkhani, R. Yarani, S. Mohammadiani, F. Amiri and K. Mansouri, Altering the characterization of nanofibers by changing the electrospinning parameters and their application in tissue engineering, drug delivery, and gene delivery systems, *Polym. Adv. Technol.*, 2021, **32**, 1924–1950.

20 N. Scharnagl and H. Buschatz, Polyacrylonitrile (PAN) membranes for ultra- and microfiltration, *Desalination*, 2001, **139**, 191–198.

21 Y. Y. Wu, R. C. Gao, S. H. Gao and M. X. Li, Poly(vinylidene fluoride)-polyacrylonitrile blend flat-sheet membranes reinforced with carbon nanotubes for wastewater treatment, *J. Appl. Polym. Sci.*, 2018, **135**, 46155.

22 N. V. Pchelova, I. A. Budkute, L. A. Shcherbina and K. Y. Ustinov, Polyacrylonitrile fiber modified by a quaternary ammonium salt, *Fibre Chem.*, 2014, **46**, 97–100.

23 M. N. Sarwar, A. Ullah, M. K. Haider, N. Hussain, S. Ullah, M. Hashmi, M. Q. Khan and I. S. Kim, Evaluating antibacterial efficacy and biocompatibility of PAN nanofibers loaded with diclofenac sodium salt, *Polymers*, 2021, **13**, 510.

24 H. Baskan, I. Esenturk, S. Dosler, A. S. Sarac and H. Karakas, Electrospun nanofibers of poly (acrylonitrile-*co*-itaconic acid)/silver and polyacrylonitrile/silver: *in situ* preparation, characterization, and antimicrobial activity, *J. Ind. Text.*, 2021, **50**, 1594–1624.

25 L. J. Villarreal-Gomez, G. L. Perez-Gonzalez, N. Bogdanchikova, A. Pestryakov, V. Nimaev, A. Soloveva, J. M. Cornejo-Bravo and Y. Toledano-Magana, Antimicrobial effect of electrospun nanofibers loaded with silver nanoparticles: influence of Ag incorporation method, *J. Nanomater.*, 2021, **2021**, 9920755.

26 S. D. Wang, Q. Ma, K. Wang and H. W. Chen, Improving antibacterial activity and biocompatibility of bioinspired electrospinning silk fibroin nanofibers modified by graphene oxide, *ACS Omega*, 2018, **3**, 406–413.

27 N. Alhusein, I. S. Blagbrough, M. L. Beeton, A. Bolhuis and P. A. De Bank, Electrospun Zein/PCL Fibrous Matrices Release Tetracycline in a Controlled Manner, Killing *Staphylococcus aureus* Both in Biofilms and Ex Vivo on Pig Skin, and are Compatible with Human Skin Cells, *Pharm. Res.*, 2016, **33**, 237–246.

28 L. Yu, S. B. Dou, J. H. Ma, Q. Gong, M. G. Zhang, X. Q. Zhang, M. Li and W. F. Zhang, An antimicrobial peptide-loaded chitosan/polyethylene oxide nanofibrous membrane fabricated by electrospinning technology, *Front. Mater.*, 2021, **8**, 650223.

29 I. E. Kochevar, C. R. Lambert, M. C. Lynch and A. C. Tedesco, Comparison of photosensitized plasma membrane damage caused by singlet oxygen and free radicals, *Biochim. Biophys. Acta*, 1996, **1280**, 223–230.

30 E. Panzarini, V. Inguscio and L. Dini, Overview of cell death mechanisms induced by rose bengal acetate-photodynamic therapy, *Int. J. Photoenergy*, 2011, **2011**, 713726.

31 J. Nakonieczna, K. Wolnikowska, P. Ogonowska, D. Neubauer, A. Bernat and W. Kamysz, Rose Bengal-Mediated Photoinactivation of Multidrug Resistant *Pseudomonas aeruginosa* Is Enhanced in the Presence of Antimicrobial Peptides, *Front. Microbiol.*, 2018, **9**, 01949.

32 M. Kurosu, K. Mitachi, J. S. Yang, E. V. Pershing, B. D. Horowitz, E. A. Wachter, J. L. W. Iii, Y. D. Ji and D. J. Rodrigues, Antibacterial activity of pharmaceutical-grade rose bengal: an application of a synthetic dye in antibacterial therapies, *Molecules*, 2022, **27**, 322.

33 M. Dabrzalska, N. Benseny-Cases, R. Barnadas-Rodriguez, S. Mignani, M. Zablocka, J. P. Majoral, M. Bryszewska, B. Klajnert-Maculewicz and J. Cladera, Fourier transform infrared spectroscopy (FTIR) characterization of the interaction of anti-cancer photosensitizers with dendrimers, *Anal. Bioanal. Chem.*, 2016, **408**, 535–544.

34 M. Y. G. Cervantes, L. Han, J. Kim, B. Chitara, N. Wymer and F. Yan, N-halamine-decorated electrospun polyacrylonitrile nanofibrous membranes: characterization and antimicrobial properties, *React. Funct. Polym.*, 2021, **168**, 105058.

35 A. N. Severyukhina, N. V. Petrova, K. Smuda, G. S. Terentyuk, B. N. Klebtsov, R. Georgieva, H. Baumler and D. A. Gorin, Photosensitizer-loaded electrospun chitosan-based scaffolds for photodynamic therapy and tissue engineering, *Colloids Surf., B*, 2016, **144**, 57–64.

36 S. M. Kamath, K. Sridhar, D. Jaison, V. Gopinath, B. K. M. Ibrahim, N. Gupta, A. Sundaram, P. Sivaperumal, S. Padmapriya and S. S. Patil, Fabrication of tri-layered electrospun polycaprolactone mats with improved sustained drug release profile, *Sci. Rep.*, 2020, **10**, 18179.

37 S. Samadi, M. Moradkhani, H. Beheshti, M. Irani and M. Aliabadi, Fabrication of chitosan/poly(lactic acid)/graphene oxide/TiO2 composite nanofibrous scaffolds for sustained delivery of doxorubicin and treatment of lung cancer, *Int. J. Biol. Macromol.*, 2018, **110**, 416–424.

38 X. H. Zong, K. Kim, D. F. Fang, S. F. Ran, B. S. Hsiao and B. Chu, Structure and process relationship of electrospun bioabsorbable nanofiber membranes, *Polymer*, 2002, **43**, 4403–4412.

39 J. Zeng, L. X. Yang, Q. Z. Liang, X. F. Zhang, H. L. Guan, X. L. Xu, X. S. Chen and X. B. Jing, Influence of the drug compatibility with polymer solution on the release kinetics of electrospun fiber formulation, *J. Controlled Release*, 2005, **105**, 43–51.

40 N. A. Peppas and J. J. Sahlin, A simple equation for the description of solute release. III. Coupling of diffusion and relaxation, *Int. J. Pharm.*, 1989, **57**, 169–172.

41 P. L. Ritger and N. A. Peppas, A simple equation for description of solute release I. Fickian and non-fickian release from non-swellable devices in the form of slabs, spheres, cylinders or discs, *J. Controlled Release*, 1987, **5**, 23–36.

42 S. Sayin, A. Tufani, M. Emanet, G. G. Genchi, O. Sen, S. Shemshad, E. Ozdemir, G. Ciofani and G. Ozaydin Ince, Electrospun nanofibers with pH-responsive coatings for

control of release kinetics, *Front. Bioeng. Biotechnol.*, 2019, **7**, 00309.

43 V. K. Gupta, A. Mittal, D. Jhare and J. Mittal, Batch and bulk removal of hazardous colouring agent Rose Bengal by adsorption techniques using bottom ash as adsorbent, *RSC Adv.*, 2012, **2**, 8381–8389.

44 P. Costa, J. Manuel and S. Lobo, Modeling and comparison of dissolution profiles, *Eur. J. Pharm. Sci.*, 2001, **13**, 123–133.

45 K. Karthikeyan, A. Babu, S. J. Kim, R. Murugesan and K. Jeyasubramanian, Enhanced photodynamic efficacy and efficient delivery of rose bengal using nanostructured poly(amidoamine) dendrimers: potential application in photodynamic therapy of cancer, *Cancer Nanotechnol.*, 2011, **2**, 95–103.

46 T. J. Silhavy, D. Kahne and S. Walker, The Bacterial Cell Envelope, *Cold Spring Harbor Perspect. Biol.*, 2010, **2**, a000414.

47 S. K. Sharma, L. Y. Chiang and M. R. Hamblin, Photodynamic therapy with fullerenes in vivo: reality or a dream?, *Nanomedicine*, 2011, **6**, 1813–1825.

48 A. F. Silva, A. Borges, C. F. Freitas, N. Hioka, J. M. G. Mikcha and M. Simoes, Antimicrobial photodynamic inactivation mediated by rose bengal and erythrosine is effective in the control of food-related bacteria in planktonic and biofilm states, *Molecules*, 2018, **23**, 2288.

49 G. Bertoloni, F. Rossi, G. Valduga, G. Jori and J. Vanlier, Photosensitizing Activity of Water-Soluble and Lipid-Soluble Phthalocyanines on *Escherichia coli*, *FEMS Microbiol. Lett.*, 1990, **71**, 149–155.

50 M. Arkoun, F. Daigle, M. C. Heuzey and A. Ajji, Antibacterial electrospun chitosan-based nanofibers: A bacterial membrane perforator, *Food Sci. Nutr.*, 2017, **5**, 865–874.

51 S. Shuai Liang, G. Zhang, J. Min, J. Ding and X. Jiang, Synthesis and antibacterial testing of silver/poly (ether amide) composite nanofibers with ultralow silver content, *J. Nanomater.*, 2014, 684251.

52 H. Y. Cui, J. Y. Lu, C. Z. Li, M. M. A. Rashed and L. Lin, Antibacterial and physical effects of cationic starch nanofibers containing carvacrol@casein nanoparticles against *Bacillus cereus* in soy products, *Int. J. Food Microbiol.*, 2022, **364**, 109530.

53 I. Buzalewicz, A. Ulatowska-Jarza, A. Kaczorowska, M. Gasior-Glogowska, H. Podbielska, M. Karwanska, A. Wieliczko, A. K. Matczuk, K. Kowal and M. Kopaczynska, Bacteria single-cell and photosensitizer interaction revealed by quantitative phase imaging, *Int. J. Mol. Sci.*, 2021, **22**, 5068.

54 F. Nakonechny, M. Barel, A. David, S. Koretz, B. Litvak, E. Ragozin, A. Etinger, O. Livne, Y. Pinhasi, G. Gellerman and M. Nisnevitch, Dark antibacterial activity of rose bengal, *Int. J. Mol. Sci.*, 2019, **20**, 3196.

55 C. A. Juan, J. M. P. de la Lastra, F. J. Plou and E. Perez-Lebena, The Chemistry of Reactive Oxygen Species (ROS) Revisited: Outlining Their Role in Biological Macromolecules (DNA, Lipids and Proteins) and Induced Pathologies, *Int. J. Mol. Sci.*, 2021, **22**, 4642.

56 T. J. Dougherty, C. J. Gomer, B. W. Henderson, G. Jori, D. Kessel, M. Korbelik, J. Moan and Q. Peng, Photodynamic therapy, *JNCI, J. Natl. Cancer Inst.*, 1998, **90**, 889–905.

57 L. Ming, K. Cheng, Y. Chen, R. Yang and D. Z. Chen, Enhancement of tumor lethality of ROS in photodynamic therapy, *Cancer Med.*, 2021, **10**, 257–268.

58 E. Skovsen, J. W. Snyder, J. D. C. Lambert and P. R. Ogilby, Lifetime and diffusion of singlet oxygen in a cell, *J. Phys. Chem. B*, 2005, **109**, 8570–8573.

59 T. Maisch, J. Baier, B. Franz, M. Maier, M. Landthaler, R. M. Szeimies and W. Baumler, The role of singlet oxygen and oxygen concentration in photodynamic inactivation of bacteria, *Proc. Natl. Acad. Sci. U. S. A.*, 2007, **104**, 7223–7228.

60 F. Sefat, T. I. Raja, M. S. Zafar, Z. Khurshid, S. Najeeb, S. Zohaib, E. D. Ahmadi, M. Rahmati and M. Mozafari, in *Micro and Nano Technologies, Nanoengineered Biomaterials for Regenerative Medicine*, ed. M. Mozafari, J. Rajadas and D. Kaplan, Elsevier, Cambridge, MA, USA, 2019, ch. 3, pp. 39–71.

© 2022 The Author(s). Published by the Royal Society of Chemistry

Environ. Sci.: Adv., 2022, **1**, 736–745 | **745**